Biointerface Research in Applied Chemistry
Open-Access Journal (ISSN: 2069-5837)

Article
Volume 14, Issue 6, 2024, 139
https://doi.org/10.33263/BRIAC146.139

Metal Complexes with Piperazine Ring Based N_2O_2 Ligands and their Biological Activity

Rishi Kant [1], Aashima Beri [1], Tanu Mittal [1], Yogesh Bhalla [1], Ritika Saini [2], Suman Maji [2,*]

[1] School of Natural Sciences, GNA University, Phagwara, Punjab, 144401, India
[2] School of Chemical Engineering and Physical Sciences, Department of Chemistry, Lovely Professional University, Phagwara, Punjab, 144411, India
* Correspondence: suman.18423@lpu.co.in;

Scopus Author ID 9244781000
Received: 11.08.2023; Accepted: 16.11.2023; Published: 10.12.2024

Abstract: This paper reports two ligands based on piperazine rings and their cobalt, copper, and zinc complexes, along with synthesis and characterization. Ligands were synthesized by direct condensation of chloroethanol and the ring-opening reaction of styrene oxide with piperazine and characterized by FT–IR, UV–Vis, mass spectrometry, and ^{1}H–NMR spectroscopic techniques. The metal complexes were synthesized in methanol and acetonitrile solvent using metal chloride salt and characterized with FT–IR, UV–Vis, mass spectrometry, ^{1}H–NMR, and electrochemical and thermal analysis. Complexes indicated a non-ionic nature in molar conductance data, and loss of coordinated solvent molecules during TGA analysis helped in the interpretation of the structure of complexes. DFT was employed to optimize the ligands and complexes. The moderate protein binding constant of the complexes with BSA favored albumin-based transportation through blood. DNA binding studies have been performed with CT-DNA, and a moderate binding constant value was observed. Molecular docking studies of selected complexes support hydrophilic interaction with BSA protein via grove binding in the DNA molecule.

Keywords: piperazine; N_2O_2 ligands; metal complexes; DFT; BSA/DNA binding; molecular docking.

1. Introduction

Piperazine ring-based heterocyclic compounds are at the center of attention for scientists owing to excellent bioactivity [1,2]. It is a six-member ring with two opposite sides of nitrogen, a weak base in nature, and soluble in common solvents [3]. Piperazine nitrogen as donor atoms and its derivatives with oxygen/nitrogen donor groups have been proven to be good ligands for forming metal complexes [4,5]. Piperazine secondary amine nitrogen can be substituted asymmetrically or symmetrically with suitable fragments [6,7]. Metal ion coordination with ligands mostly enhances biological activities, and thus, piperazine-based ligands become important and can be easily designed for potential applications [8,9].

Many marketed drugs contain piperazine as a core figure and have been considered a privileged structure in the field of medicinal chemistry. Due to variable binding properties, it becomes a molecular backbone and selectively binds with various biomolecules [10]. Based on this structure, an array of molecules have been screened and found promising applications as antimicrobial, anticancer, antioxidants, and antidepressants [11]. Substituted piperazine ring-based ligands can potentially bind one or two metal ions (Figure 1) in boat and chair conformations [12,13].

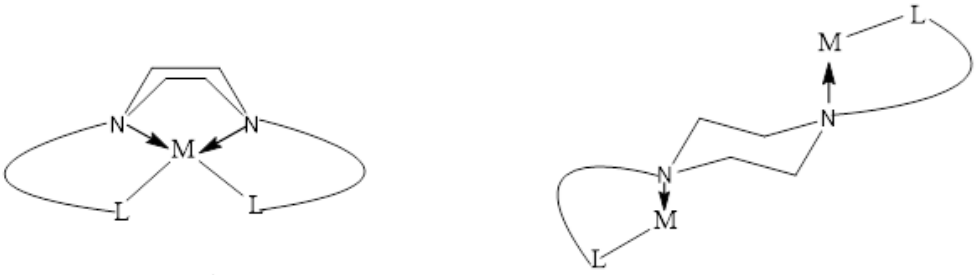

(a) **(b)**

Figure 1. Two binding modes of piperazine ring-based ligands **(a)** monometallic; and **(b)** bimetallic.

Many biomolecules containing heterocyclic systems have been known to interact directly or indirectly with metal ions in our bodies [14]. This encourages using these heterocycles as the primary component of ligands that bind to various metal ions for various applications [15]. Bioactivities of these piperazine-based complexes toward specific target receptors such as BSA protein or DNA molecules have been explored significantly for behaving as potential drug molecules via spectroscopic methods [16-18]. The anticancer potential of piperazine ring-based metal complexes in terms of cytotoxicity has also attracted attention, and these DNA binding mechanisms of complexes have been proved by either intercalation or groove binding [19-22].

2. Materials and Methods

All the chemicals used in the study were purchased from Molychem and Loba Chemie India and used as received. UV–Vis spectra were recorded on Shimadzu UV–1800, having a wavelength of 200-800 nm. FT–IR 8400 spectrometer (Shimadzu) was used to record IR spectra. ^{1}H NMR spectra were recorded from NMR spectrometer (Brucker Advance II 400 MHz) in $CDCl_3$/d^6–DMSO. Mass spectra were recorded from a mass spectrometer (XEVO G2-XS QTOF). The synthetic scheme and structure of ligands are given in Figure 2, whereas the proposed structure of complexes is given in Figure 3.

2.1. Synthesis of ligands.

2.1.1. Synthesis of 1,4-bisethanol piperazine (H_2L1).

In 30 ml of n-propanol, piperazine (20 mmol, 1.72 g) was dissolved and mixed slowly with a solution of chloroethanol (24 mmol, 3.22 g); in 10ml of n-propanol was mixed slowly with constant shaking. The resultant mixture was then constantly refluxed for one hour, and 5.35 g of potassium carbonate (40 mmol) was added. Further refluxing was done for 7 hours under 65-75°C, and reaction progress was checked by doing TLC with a solvent mixture of chloroform and methanol at 7:3. Then, the mixture was cooled for 2 hrs and filtered. The filtrate was allowed to stand for 3-4 days, and a white crystalline solid appeared. This solid product was then filtered and washed. Recrystallization was done in hot methanol. Appearance *solid shining white*, yield 75%, UV–Vis (λ_{max}, nm) 211, FT–IR (ν, cm^{-1}) 2915 (C–H str.), 1302 (C–C str.), 1328 (C–N str.), 3124 (O–H str.) ^{1}H NMR (DMSO, δ, ppm) 4.37 (2H, –CH_2, triplet), 2.50 (4H, –CH_2, triplet), 3.45 (2H, –CH_2, triplet), Mass (m/z, $M+H^+$) 175.

2.1.2. Synthesis of bis-(1-phenylethanol) piperazine (H_2L2).

In the 25 ml of ethanol, 1.72 g (20 mmol) of piperazine was dissolved, and 4.80 g (40 mmol) of styrene oxide was mixed slowly with constant shaking. The refluxing of the resultant mixture was done for five hrs, and a white-colored precipitate was separated. This product was then filtered, dried, and recrystallized in ethanol. The whole reaction was monitored by doing TLC in small intervals. Appearance *solid off white*, yield 84%, UV–Vis (λ_{max}, nm) 212, 252, FT–IR (ν, cm^{-1}) 2923 (C–H str.), 1319 (C–N str.), 3369 (O–H str.), ^1H NMR ($CDCl_3$, δ, ppm) 2.87 (2H, $–CH_2$, doublet), 2.78 (4H, $–CH_2$, triplet), 3.98 (1H, –CH, triplet), 7.27 (3H, Ar–H, triplet), 7.16 (2H, Ar–H, doublet), Mass (m/z $M+H^+$) 327.

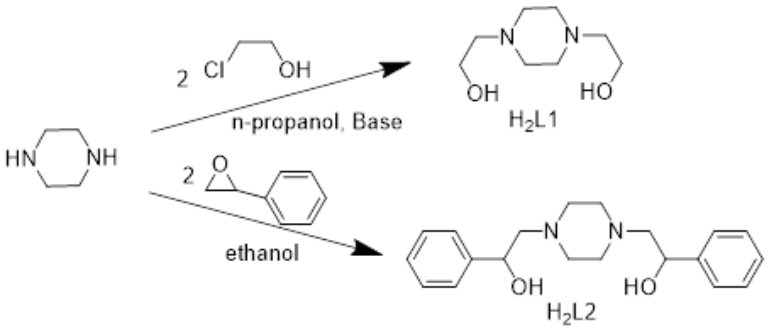

Figure 2. Synthetic scheme and structure of ligands H_2L1-2.

2.2. Synthesis of metal complexes.

2.2.1. Synthesis of $[CoL1(H_2O)_2]$ (CoL1).

0.21 g (1.29 mmol) of ligand H_2L1 was added in 25 ml of methanol, and to this solution, 0.22 g (1.29 mmol) cobalt chloride hexahydrate was mixed. The refluxing of the resultant mixture was done for three hrs under 50-60°C. The resultant mixture was allowed to stand and then filtered. The filtered solution was kept undisturbed for 6-8 days. In the end, light blue precipitates were obtained by removing the mother liquor, and the obtained precipitates were washed in methanol and dried in a vacuum desiccator. Appearance *solid light blue*, yield 62%, UV–Vis (λ_{max}, nm) 209, 257, FT–IR (ν, cm^{-1}) 436 (Cu–O vib.), 495 (Cu–N vib.), 1326 (C–N str.), 3122 ($M–OH_2$ str.), Mass (m/z) 139, 146, 175, 232, 259, 268.

2.2.2. Synthesis of $[Co_2(L2)(CH_3OH)_4(Cl)_2(H_2O)_2]$ (Co_2L2).

A similar procedure was applied as described for CoL1. Appearance *solid light blue*, yield 62%, UV–Vis (λ_{max}, nm) 212, 255, UV–Vis (λ_{max}, nm) 212, 255, FT–IR (ν, cm^{-1}) 429 (Cu–O vib.), 507 (Cu–N vib.), 1300 (C–N str.), 1640 (C=C str.), 3020 (C–H str.), 3279 ($M–OH_2$ str.), Mass (m/z) 309, 327, 415, 447, 567, 687.

2.2.3. Synthesis of $[Cu_2(L2)(CH_3CN)Cl_2(H_2O)_5]$ (Cu_2L2).

A similar procedure was applied to CoL1, with acetonitrile as a solvent and copper chloride as a metal ion source. Appearance *solid light yellow*, yield 64%, UV–Vis (λ_{max}, nm) 211, 256, FT–IR (ν, cm^{-1}) 404 (Cu–O vib.), 521 (Cu–N vib.), 1329 (C–N str.), 1555 (C=C str.), 2920 (C–H str.), 3319 ($M–OH_2$ str.), Mass (m/z) 189, 207, 220, 253, 262, 327.

2.2.4. Synthesis of $[Zn_2(L2)(CH_3CN)_2Cl_2(H_2O)_4]$ (Zn_2L2).

A similar procedure was applied for the described CoL1 with acetonitrile as a solvent and zinc chloride as a metal ion source. Appearance *solid white*, yield 63%, UV–Vis (λ_{max}, nm) 211, 257, FT–IR (ν, cm^{-1}) 429 (Cu-O vib.), 465 (Cu-N vib.), 1241 (C-N str.), 1554 (C=C str.), 3035 (C-H str.), 3380 (M-OH_2 str.), ^1H NMR (DMSO, δ, ppm) 3.31(4H, –CH_2, triplet), 3.99(2H, –CH_2, doublet), 4.5(1H, –CH, triplet), 7.27(2H, Ar–H, doublet), 7.40(3H, Ar–H, triplet) Mass (m/z) 291, 309, 327, 453, 473, 679.

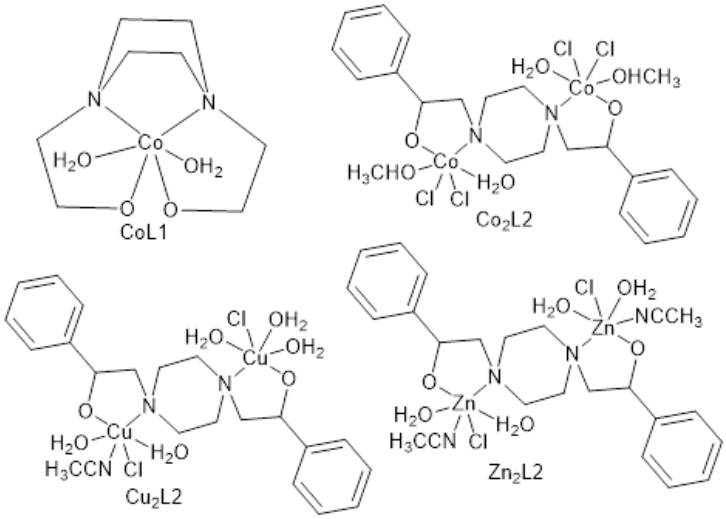

Figure 3. Structure (proposed) of complexes CoL1, Co_2L2, Cu_2L2, Zn_2L2.

3. Results and Discussion

3.1. UV–Vis analysis.

Ligand H_2L1 showed a single maximum wavelength peak at 211 nm (Ɛ = 2090 $Lmol^{-1}cm^{-1}$), while H_2L2 showed two peaks at 212 (Ɛ = 2110 $Lmol^{-1}cm^{-1}$) and 252 (Ɛ = 230 $Lmol^{-1}cm^{-1}$) nm. These peaks indicated the presence of n→σ* type transition in ligand H_2L1 while n→σ* and π→π* type of electronic transitions in ligand H_2L2. In the first ligand, there was no π electron system, so no peak was observed for the unsaturated system. At the same time, ligand H_2L2 showed an absorption peak at a higher wavelength (252nm) due to the presence of a benzene ring. The metal binding was observed from the UV–Vis analysis from the change in the intensity and 3-4 nm shift in the wavelength (λ_{max}) from that of ligands absorption (Figure 4).

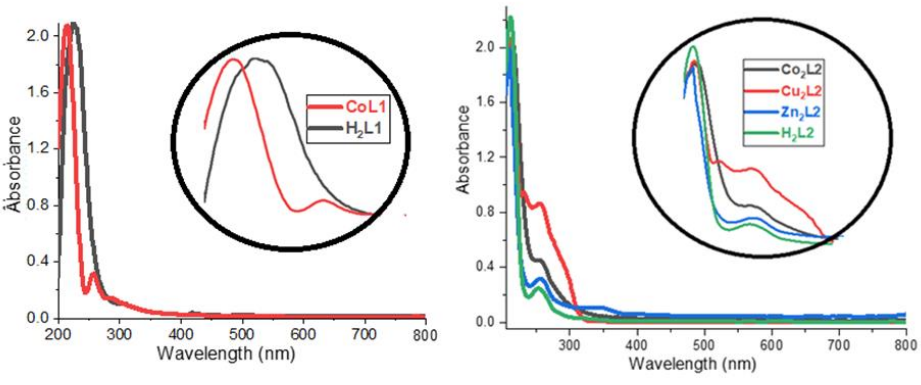

(a) **(b)**

Figure 4. UV-Vis absorption spectra of H_2L1, H_2L2 (ligands) and CoL1, Co_2L2, Cu_2L2, Zn_2L2 (complexes).

3.2. FT–IR analysis.

In the ligands, H_2L1-2, a band near 3350-3250 cm^{-1} appeared for the hydroxy group, i.e., O–H stretching. 1440 cm^{-1} peak in H_2L2 indicated the presence of C=C stretching of the aromatic ring, which was absent in ligand H_2L1 due to the absence of unsaturation. Other C–H and C–N bond stretching also appeared between 1300-1360 cm^{-1} and 2930-3100 cm^{-1}. FT–IR data has been used to explain the binding behavior of metal complexes with the ligands due to the lack of X-ray data [23,24]. Absorption bands in the range 405-437 cm^{-1} and 495-520 cm^{-1} were assigned to Metal–Oxygen and Metal–Nitrogen vibrations to ascertain the new bond formation between metal ions and ligands. Also, the absorption peaks in the range 3200-3380 cm^{-1} in these complexes validated the presence of coordinated or lattice water [25]. FT–IR data of ligands and complexes with selected bond frequencies have been described in Table 1.

Table 1. FT–IR data (in cm^{-1}).

Code	ν O–H/M–OH_2	ν M–O	ν M–N	ν C=C(Ar)	ν C–N	ν C–H
H_2L1	3124	-	-	-	1328	2915
H_2L2	3369	-	-	1440	1319	2923
CoL1	3122	436	495	-	1329	3138
Co_2L2	3279	429	507	1643	1300	3020
Cu_2L2	3319	404	521	1555	1325	2920
Zn_2L2	3380	429	465	1554	1241	3035

3.3. Mass spectral analysis.

ESI mass under +ve ionization mode has been used to analyze the mass spectra of ligands and complexes. The fragmentation pattern of the complexes supported the binding of metal ions with that of ligands and other coordinating solvent molecules [26,27]. Experimental and calculated isotopic distribution patterns were also in favor of the given structure of complexes. In the case of ligand H_2L1, the peak of molecular ion $[M+H^{\cdot}]^+$ was observed at m/z 175, representing molecular mass. Very low fragmentation was observed due to the small ligand skeleton, as indicated in mass spectra, which have a dominant molecular ion peak. A peak at m/z 219 has been represents a ligand coupled with an ethyl alcohol fragment, whereas a peak at m/z 157 represents the loss of water, a common fragmentation of alcohols (Figures 5 and 6).

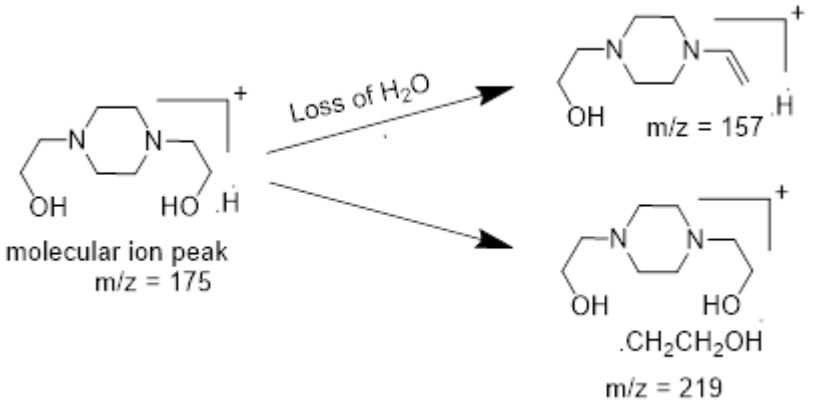

Figure 5. Fragmentation pattern of ligand H_2L1.

Ligand H_2L2 also showed a molecular ion peak at m/z 327 $[M+H^{\cdot}]^+$ representing molecular mass. Similar to ligand H_2L1, much less fragmentation was observed due to the small ligand skeleton, as indicated in mass spectra, having a dominant molecular ion peak.

Water loss was observed at m/z 309, a common fragmentation of alcohols. Direct loss of one arm of ligand or styrene fragment from m/z 309 was observed at m/z 207, followed by the loss of water indicated at m/z 189. (Figures 7 and 8).

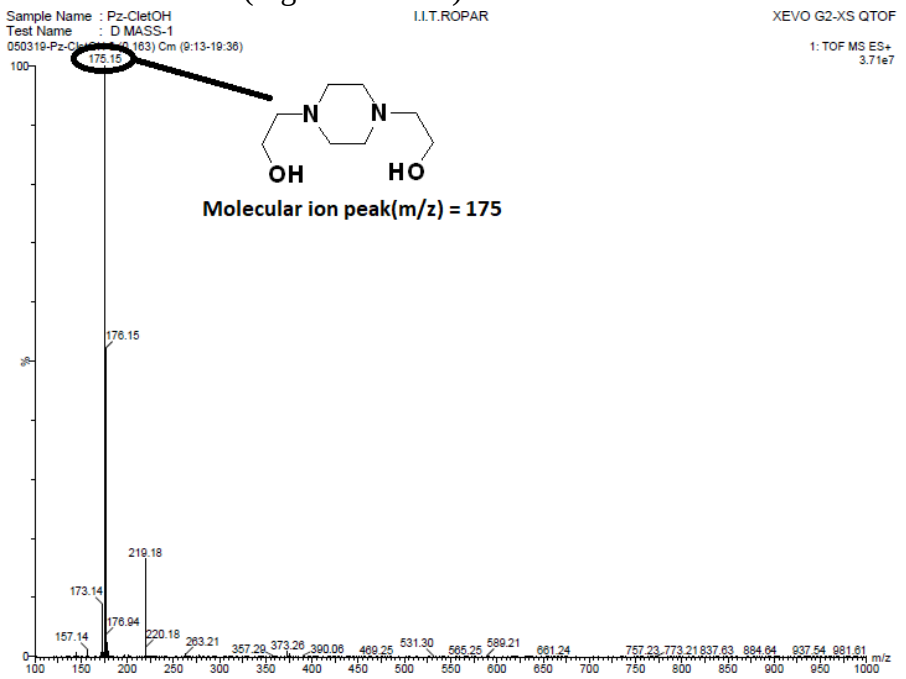

Figure 6. Mass spectra of H2L1.

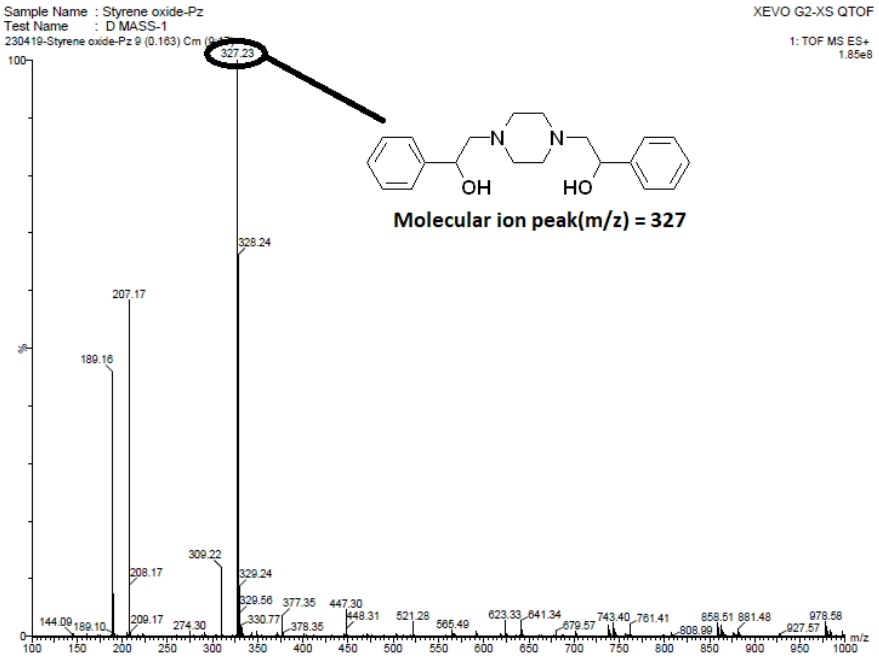

Figure 7. Mass spectra of H_2L2.

In the mass spectra of complex $[Co(L1)(H_2O)_2]$ (Figure S1), peaks at m/z 268 have been assigned for the molecular formula. The loss of coordinated water molecules was indicated by a peak at m/z 232. Complete loss of coordination resulted in free ligands observed at m/z 175, which can be obtained from m/z 268 and 232. Loss of two water from free ligand was observed at m/z 139, whereas loss of ethylene arm corresponded to m/z 146 (Figure 9).

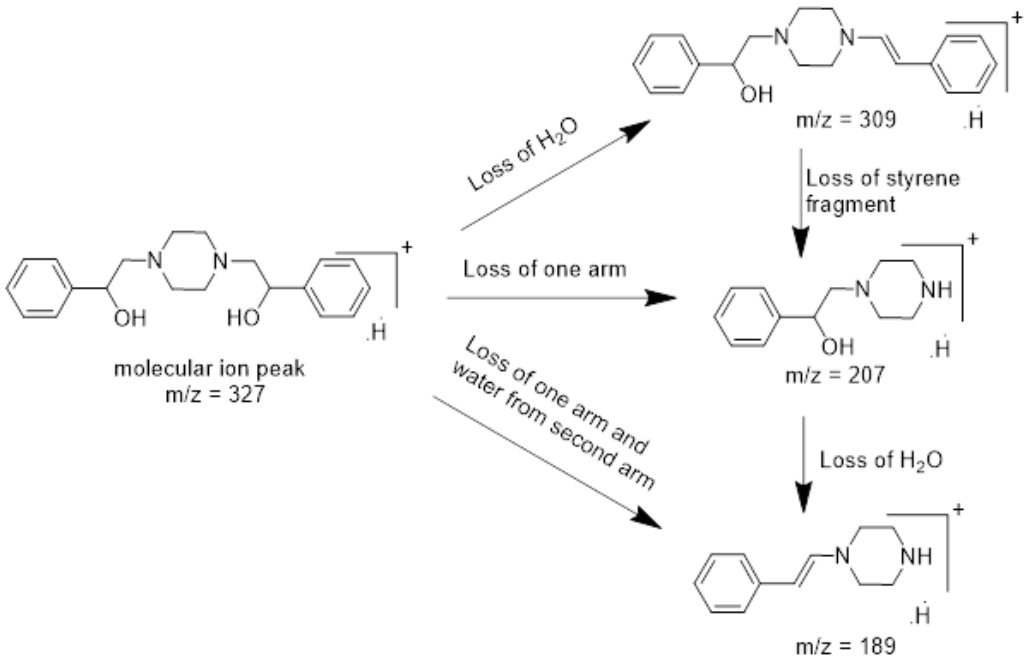

Figure 8. Mass fragmentation pattern of ligand H_2L2.

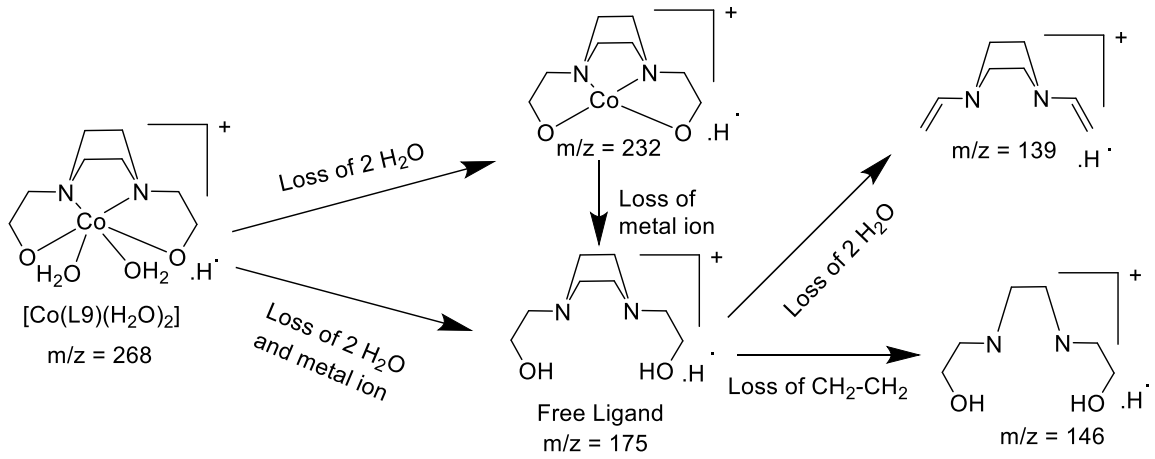

Figure 9. Mass fragmentation pattern of $[Co(L1)(H_2O)_2]$.

In the mass spectra of complex $[Co_2(L2)Cl_4(H_2O)_2(CH_3OH)_2]$ (Figure S2), peak at m/z 687 have been assigned for molecular formula. Loss of one chloro, two water, and two methanol coordinated to metal ions was observed at m/z 567. From m/z 567, loss of two chloro was observed at m/z 447, and ultimately, loss of two metal ions resulted in free ligand observed at m/z 327. In another way, the loss of two styrene epoxide residues in series from m/z 687 resulted in m/z at 567 and 447. From m/z 447, a loss of methanol was observed at m/z 415 (Figure 10).

In the mass spectra of complex $[Cu_2(L2)Cl_2(CH_3CN)(H_2O)_5]$ (Figure S3), the peak at m/z 327 represented the molecular formula of the complex by taking charge as +2. Loss of one water, one acetonitrile, and two chloro coordinated to metal ion was observed at m/z 262. Loss of water molecules in series was observed at m/z 253, 235, and 189. In another way, the loss of one water, all chloro and phenyl ring of ligand was observed at m/z 207 (Figure 11).

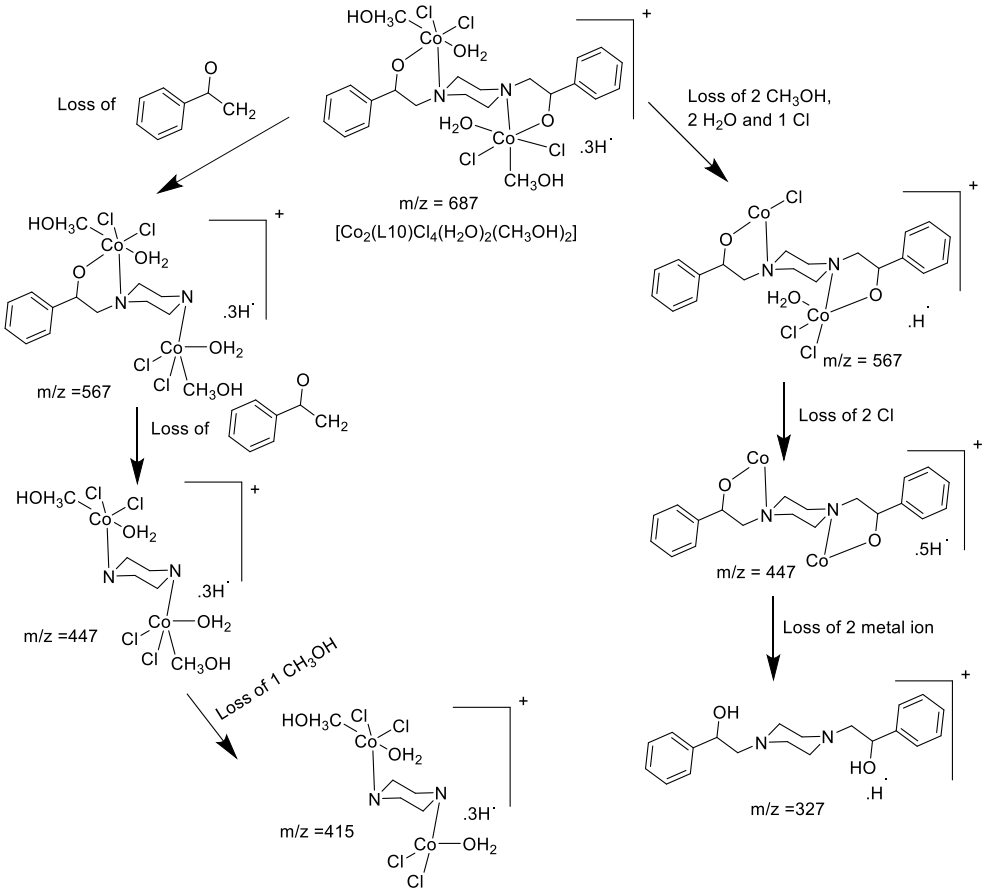

Figure 10. Mass fragmentation pattern of $[Co_2(L2)Cl_4(H_2O)_2(CH_3OH)_2]$.

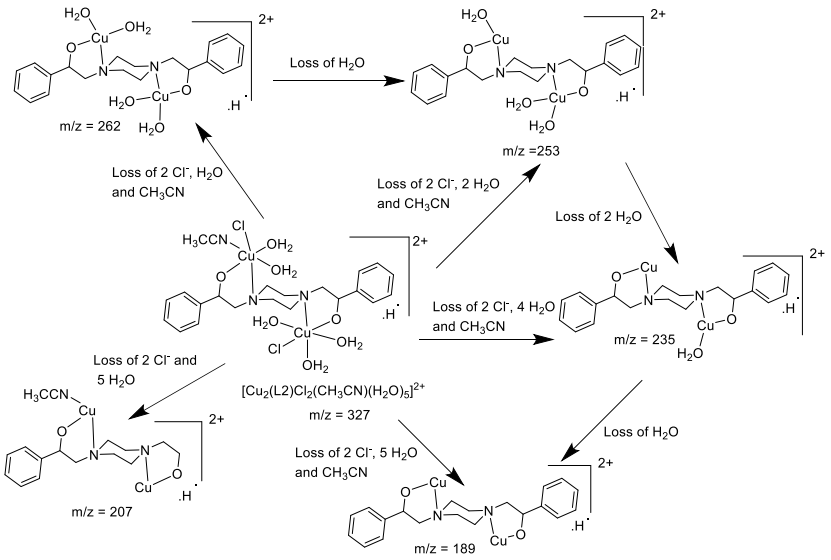

Figure 11. Mass fragmentation pattern of $[Cu_2(L2)Cl_2(CH_3CN)(H_2O)_5]$.

Peak at m/z 679 in the mass spectra of complex represented molecular formula as $[Zn_2(L2)Cl_2(CH_3CN)_2(H_2O)_4]$ (Figure S4)of the complex. Loss of two chloro, three water, and one acetonitrile coordinated to metal ion was observed at m/z 473. From m/z 473, loss of one water was observed at m/z 453, and ultimately, loss of two metal ions resulted in a free ligand observed at m/z 327 (Figure 12).

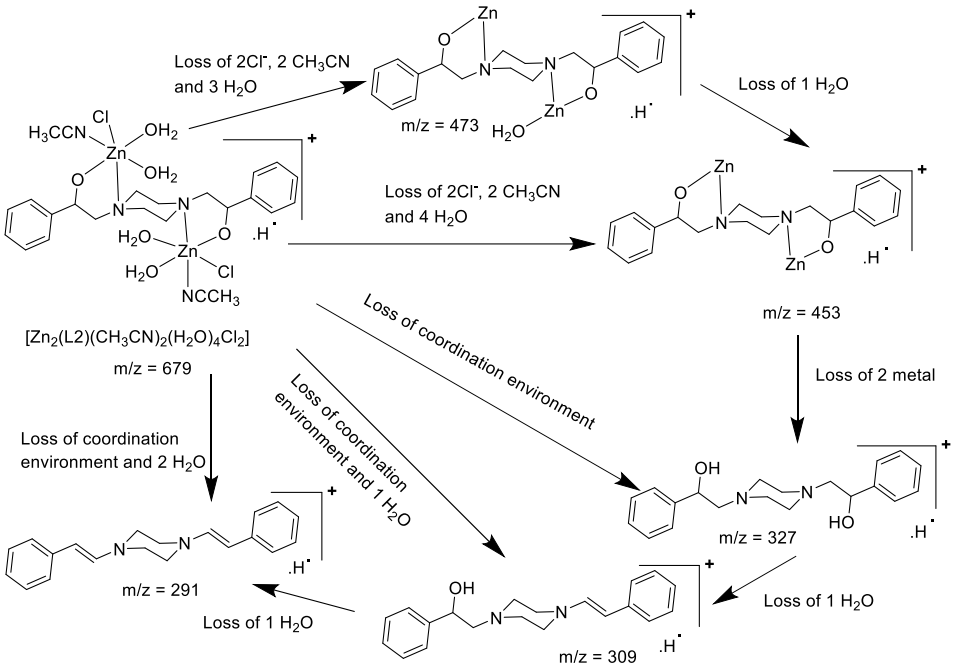

Figure 12. Mass fragmentation pattern of $[Zn_2(L2)Cl_2(CH_3CN)_2(H_2O)_4]$.

3.4. ^{1}H NMR spectral analysis of zinc complex.

In the ^{1}H NMR spectra of the zinc complex as compared to ligand H_2L (Figure S5, S6), protons experienced slight downfield due to increased conjugation of aromatic rings with a hydroxy group and electronic de-shielding of the sigma skeleton [28,29]. Aromatic proton peaks are shifted from 7.16, 7.25 ppm to 7.27, 7.40 ppm. While that of -CH_2 protons peaks 2.79, 2.89 ppm are shifted to 3.31, 3.99 ppm. CH proton experienced greater de-shielding due to the electronegative environment of oxygen and nitrogen coordination with metal, and the peak was shifted from 3.98 to 4.50 ppm [30].

3.5. Molar conductance measurements.

Conductance measurements of metal complexes have been exploited to get an idea of composition by calculating the number of ions in the electrolytic solution. Molar conductance data have also been utilized to predict complexes' ionic or non-ionic behavior [31]. The molar conductance value obtained for metal complexes suggests a non-ionic nature in DMSO and water (Table 3), which favored the structures of complexes. Thermogravimetric analysis has been further used to support the above observation.

3.6. Thermogravimetric analysis.

In the TGA graph of $[Cu_2(L2)Cl_2(CH_3CN)(H_2O)_5]$ and $[Zn_2(L2)(CH_3CN)_2(H_2O)_4Cl_2]$, loss of acetonitrile/water coordinated to metal ion was observed in the first derivative peak in the temperature range 160-180°C. Ligand decomposition in the major broad peak occurred in the temperature range 310-370°C (Figure 13). Ash content calculation supported the existence of two metals changing to metal oxide ash in the case of Cu_2L2 and Zn_2L2 [32,33].

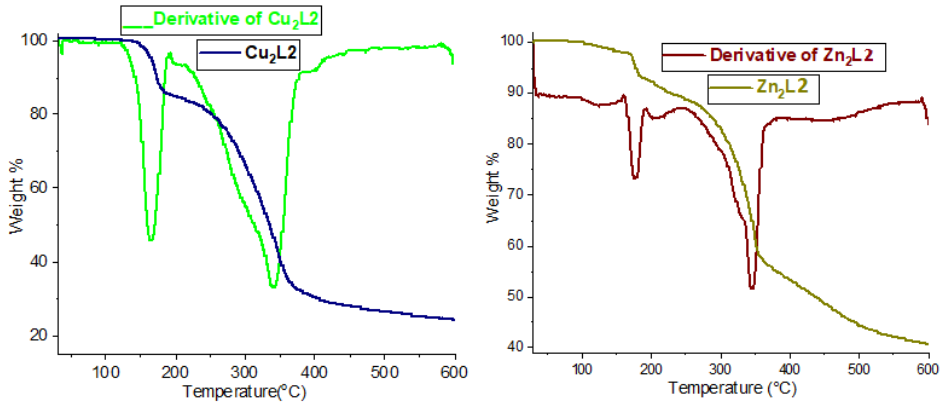

Figure 13. TGA and first derivative of Cu_2L2 and Zn_2L2.

3.7. Antibacterial activity.

Antibacterial activity of all the ligands and complexes was screened against two bacterial strains, *E. coli* and *S. aureus*, using the agar well diffusion method. In this process, compounds were dissolved in DMSO (5 mg/ml), and 100µL of each sample was loaded on a 9 mm diameter well of MHA medium with bacterial culture. The total incubation was carried out for 24 hrs at 37°C. The activity was measured in terms of the zone of inhibition by calculating the nearby area of effect. Calculations were carried out at least three times for minimum deviation (Table 2). The result of the antibacterial study indicated ligands H_2L1, H_2L2, and CoL1 were not very active, but Co_2L2, Cu_2L2, and Zn_2L2 showed higher activity as compared to standard amikacin as well as ligand H_2L2 against *E. coli* (Table 2).

Table 2. Antibacterial activity: zone of inhibition (in mm) ± standard deviation

Sr. No	*E. coli*	*S. aureus*
H_2L1	7.15 ± 0.36	-
CoL1	7.15 ± 0.36	5.12 ± 0.36
H_2L2	6.55 ± 0.58	4.11 ± 0.25
Co_2L2	26.88 ± 0.58	12.44 ± 0.25
Cu_2L2	27.22 ± 0.58	24.55 ± 0.25
Zn_2L2	25.77 ± 0.58	20.34 ± 0.25
Amikacin	22.40 ± 0.40	23.73 ± 0.66
DMSO	-	-

3.8. BSA binding studies.

UV-Vis absorption spectroscopy has been used to examine the binding interactions of complexes with serum protein (BSA). 1M solution of BSA and 50 µM solution of complexes were prepared in tris buffer solvent (0.1M, pH 7.4). Titration spectra were recorded by tanking increasing concentrations of BSA vs. fixed concentration of metal complexes. Binding constants were calculated based on the relationship between absorbance (at 273 nm) and concentrations of BSA solution (1/[BSA] and 1/[A-A_0]) by using the procedure reported previously [18,34]. Linear fit curves (Figure S7-S11) that were utilized to determine the binding constants have been presented in the supplemental file. Binding constant value indicated moderate binding of complexes with BSA protein, which favored serum protein's role as a transporter for drug delivery (Figure 14).

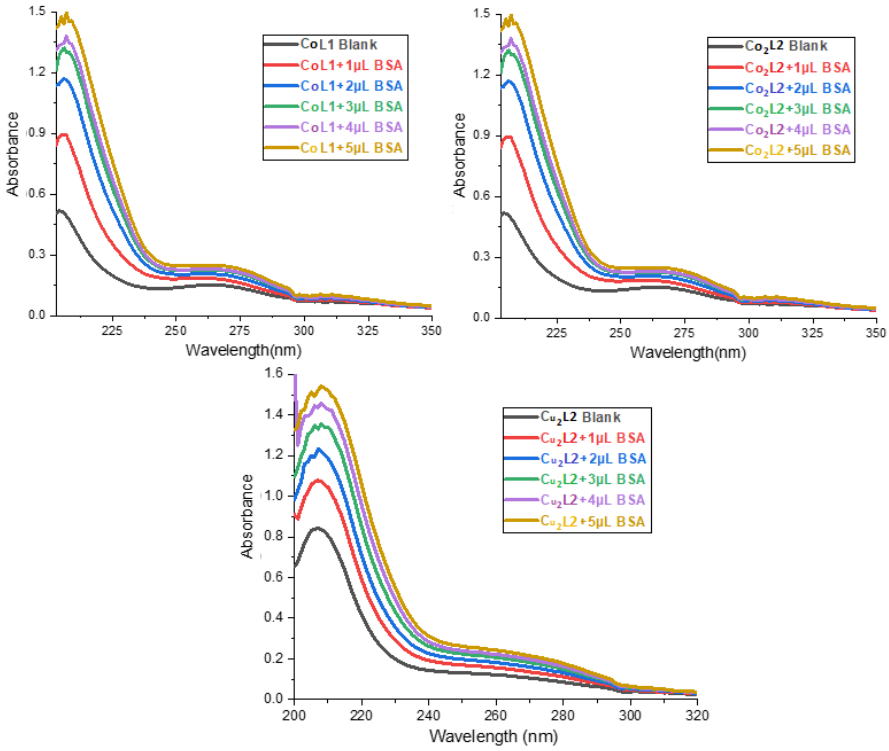

Figure 14. UV-Vis titration of complexes CoL1, Co_2L2, Cu_2L2 with BSA.

Table 3. Molar conductance ($Ohm^{-1}cm^2mol^{-1}$) and BSA/DNA binding constants K_b (M^{-1}).

Code	Molar Conductance		BSA Binding Constant	DNA Binding Constant
	DMSO	Water		
CoL1	46.0	112	1.50×10^2	1.80×10^2
Co_2L2	39.7	75	0.86×10^2	2.27×10^2
Cu_2L2	47.7	110	0.54×10^2	2.38×10^2
Zn_2L2	45.4	80	-	-

3.9. DNA binding studies.

Following BSA binding, DNA binding studies have been performed to check the binding interaction with DNA. CT-DNA solution (3 mg/ml) has been prepared in tris buffer (0.1M, pH 7.4), and the concertation was determined from 260 nm (absorbance) and 6600 (extinction coefficient) reported in the literature [21]. Titration spectra were recorded by tanking increasing concentrations of CT DNA vs fixed concentration of metal complexes (Figure 15). By plotting the graph $1/[A-A_0]$ vs. $1/[DNA]$, binding constants were calculated, and the value indicated moderate interaction with DNA. Theoretical docking studies have visualized the mechanism for binding interactions.

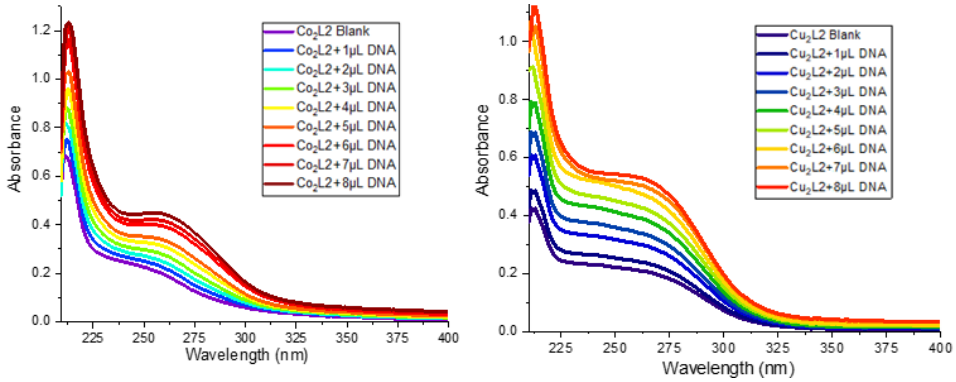

Figure 15. UV-Vis titration of complexes Co_2L2 and Cu_2L2 with BSA.

3.10. DFT calculations.

Ligands were optimized using Orca 4.0.1.2 software package [35] to find the equilibrium lowest energy structure with Hybrid functional B3LYP/6-31G(2d,2p). Metal ions binding with ligands might impose the modification in geometry, and thus, all the complexes were also theoretically optimized. Proposed complexes CoL1 and Cu_2L2 were optimized geometrically using DFT calculations with the basis set as Lan2DZ. Structures of optimized ligand and complex have been represented in Figure 16-19, and cartesian coordinates are given in the supplementary file (Table S1-S4).

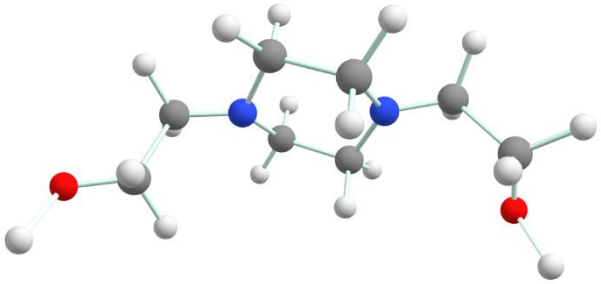

Figure 16. Optimized structure of H_2L1.

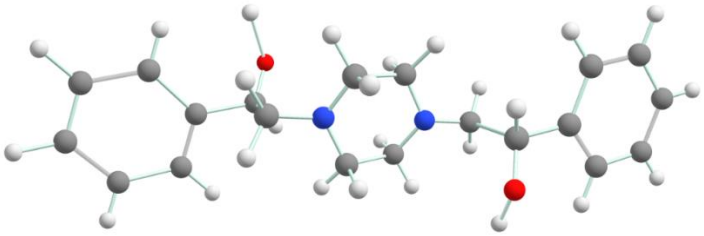

Figure 17. Optimized structure of H_2L2.

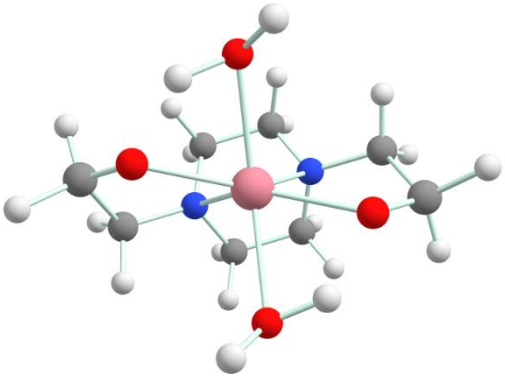

Figure 18. Optimized structure of CoL1.

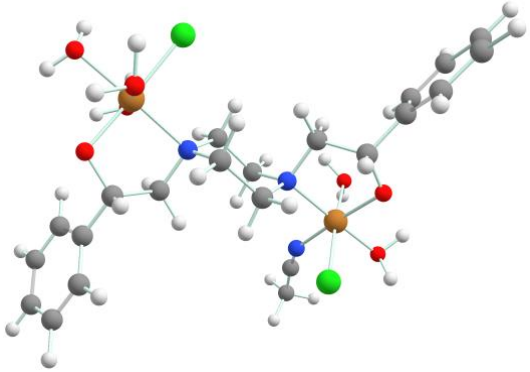

Figure 19. Optimized structure of Cu_2L2.

3.11. Molecular docking studies.

To visualize the binding interactions, molecular docking of metal complexes CoL1 and Cu_2L2 has been performed to demonstrate available binding sites in the BSA protein. The protein sequence was obtained from the PDB (code: 3V03) source. Grid was generated (size 2800Å) with 0.7Å spacing from Auto-dock tool, and docking was performed with Auto-dock Vina [36]. Complex CoL1 binds with LYS177, SER191, and TYR156 through H-bond interaction with the nearby environment of ARG194, ARG198, ARG217, LYS187, GLU291, and HIS287 residue (Figure 20) and showed binding affinity of -5.1Kcal/mol. Whereas complexes Cu_2L2 binds with ASP1, HIS67, GLU243, LYS242, and LYS239 through polar interaction in a nearby environment of ARG194, LYS221, ALA290, GLU291, TYR156, GLU152, and TYR194 residues (Figure 21) and showed binding affinity of -7.5Kcal/mol.

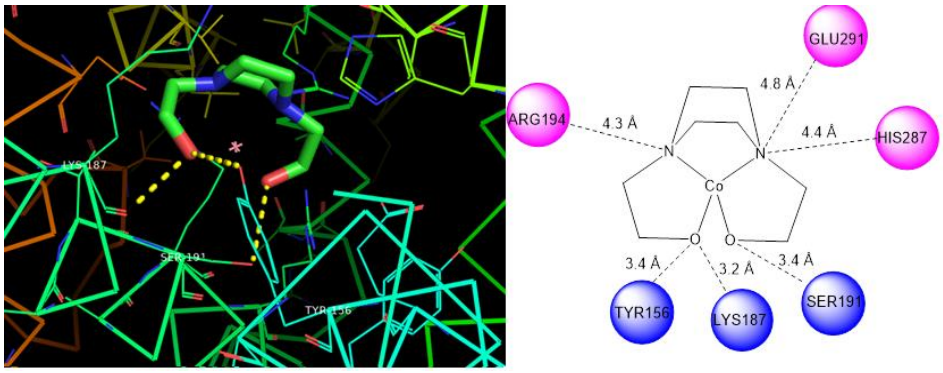

Figure 20. Docked pose of CoL1 with BSA along with structural analysis.

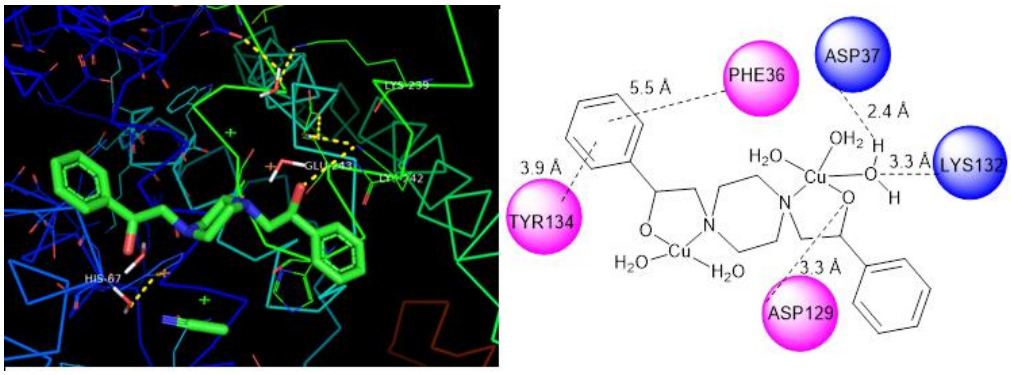

Figure 21. Docked pose of Cu_2L2 with BSA along with structural analysis.

These molecular docking studies have been further explored to check binding behavior with DNA. The DNA source was obtained from Protein Data Bank (code: 1BNA), and coordinate water molecules were removed before docking for complexes to become unsaturated. The docking result of CoL1 indicated that the complex shows interaction with only one strand of DNA through Adenine (DA5) and Guanine (DG4) with ligand oxygen atoms (Figure 22). In complex Cu_2L2, both the DNA strands are locked with metal ion interaction with Adenine DA5, DA17, and ligand oxygen atom interaction with Guanine DG4 (Figure 23).

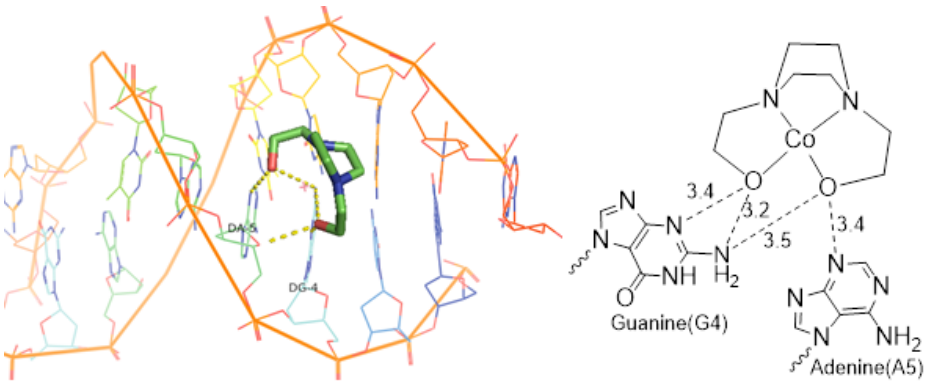

Figure 22. Theoretical binding pose of CoL1 with DNA along with structural interpretation.

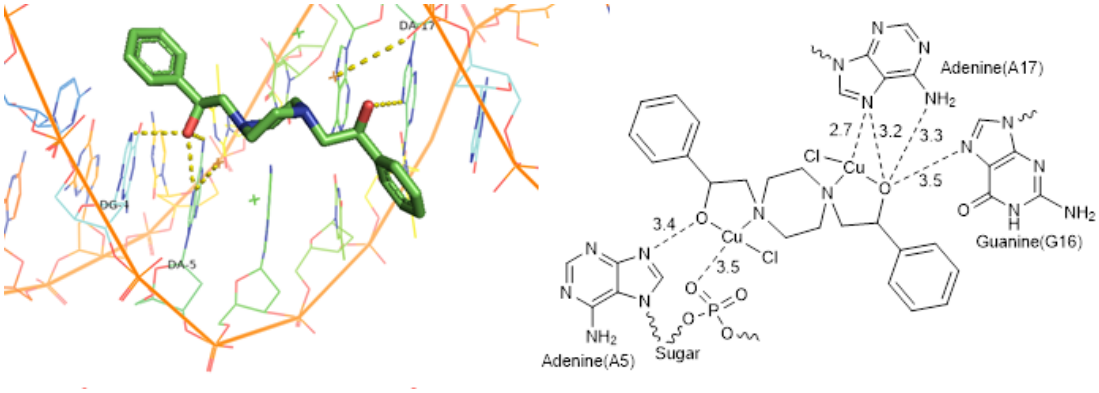

Figure 23. Theoretical binding pose of Cu_2L2 with DNA along with structural interpretation.

4. Conclusions

Two-based ligands, one with a complete sigma electron backbone and the other with a benzene ring, were synthesized and characterized. The proposed structure of complexes has been supported based on findings of UV–Vis, FT–IR, mass spectra, molar conductance, and thermal studies. IR data indicated metal binding with a ligand based on M–O, and M–N vibration frequencies in the range 404-436 and 464-521cm^{-1}. Molar conductance indicated the non-electrolytic nature of complexes, and the loss of coordinated solvent molecules was assisted by TGA curves. Loss of methanol occurred early in the 60-70°C range, whereas water and other coordinated molecules were lost after 100°C, which justifies the proposed structures of complexes. Antibacterial activity suggested copper and cobalt complexes of H_2L2 are more active against *E. coli* than the ligands and standard amikacin. The BSA and DNA binding studies showed that complexes moderately bind to the target receptor with a binding constant of 10^2 M^{-1}. Molecular docking studies revealed that complex CoL1 shows hydrophilic environment interaction with BSA whereas complex Cu_2L2 shows both hydrophobic and hydrophilic interaction owing to an aromatic ring in the ligand skeleton. DNA docking revealed that both complexes CoL1 and Cu_2L2 show affinity toward Adenine and Guanine residue and are groove binders.

Funding

This research received no external funding.

Acknowledgments

Presented in 4th International Conference on "Recent Advances in Fundamental and Applied Sciences" (RAFAS-2023)" on March 24-25, 2023, Organized by the School of Chemical Engineering and Physical Sciences, Lovely Professional University, Punjab, India. A special thanks to Ms. Jyoti Awasthi for moral support. Advanced characterization of complexes was not performed due to the impact of COVID-19 on the research work.

Conflicts of Interest

The authors declare no conflict of interest.

References

1. Mondal, K.; Dey, A.; Mistri, S. Aminoethylpiperazine Based Metal Schiff Base Complexes: Catalytic and Biological Activities. *Comments Inorg. Chem.* **2022**, *43*, 357-381, https://doi.org/10.1080/02603594.2022.2140146.
2. Kant, R.; Maji, S. Synthesis, characterization and biological evaluation of piperazine embedded copper complexes. *Inorganica Chim. Acta* **2023**, *552*, 121515, https://doi.org/10.1016/j.ica.2023.121515.
3. Khalili, F.; Henni, A.; East, A.L.L. pK_a Values of Some Piperazines at (298, 303, 313, and 323) K. *J. Chem. Eng. Data* **2009**, *54*, 2914-2917, https://doi.org/10.1021/je900005c.
4. Ragab, M.S.; Shehata, M.R.; Shoukry, M.M.; Haukka, M.; Ragheb, M.A. Oxidative DNA cleavage mediated by a new unexpected [Pd(BAPP)][$PdCl_4$] complex (BAPP= 1,4-bis(3-aminopropyl)piperazine): crystal structure, DNA binding and cytotoxic behavior. *RSC Adv.* **2022**, *12*, 1871-1884, https://doi.org/10.1039/d1ra07793g.
5. Ragab, M.S.; Soliman, M.H.; Shehata, M.R.; Shoukry, M.M.; Ragheb, M.A. Design, synthesis, spectral characterization, photo-cleavage, and in vitro evaluation of anticancer activities of new transition metal complexes of piperazine based Schiff base-oxime ligand. *Appl. Organomet. Chem.* **2022**, *36*, e6802, https://doi.org/10.1002/aoc.6802.
6. Santes, V.; Gómez, E., Zárate, V.; Santillan, R.; Farfán, N.; Rojas-Lima, S. Synthesis of new homochiral 2,3-dialkylpiperazines derived from (R)-(−)-phenylglycinol. *Tetrahedron: Asymmetry* **2001**, *12*, 241-247, https://doi.org/10.1016/S0957-4166(01)00036-2.
7. Hoarau, M.; Vanichtanankul, J.; Srimongkolpithak, N.; Vitsupakorn, D.; Yuthavong, Y.; Kamchonwongpaisan, S. Discovery of new non-pyrimidine scaffolds as *Plasmodium falciparum* DHFR inhibitors by fragment-based screening. *J. Enzyme Inhib. Med. Chem.* **2021**, *36*, 198-206, https://doi.org/10.1080/14756366.2020.1854244.
8. Peng, X.; Chen, Q.; Han, B.; Zhang, H.; Li, J.; Zhang, Q. Chapter 13 - Applications of piperazine scaffold in drug design. In Privileged Scaffolds in Drug Discovery, Academic Press, **2023**, 273-299, https://doi.org/10.1016/B978-0-443-18611-0.00018-8.
9. Das, P.; Rajput, S.S.; Das, M.; Laha, S.; Choudhuri, I.; Bhattacharyya, N.; Das, A.; Samanta, B.C.; Alam, M.M.; Maity, T. Easy, selective and colorimetric detection of Zn(II), Cu(II), F^- ions by a new piperazine based Schiff base chemosensor along with molecular logic gate formation and live cell images study. *J. Photochem. Photobiol. A: Chem.* **2022**, *427*, 113817, https://doi.org/10.1016/j.jphotochem.2022.113817.
10. Zhang, H.; Wang, Y.; Wang, Y.; Li, X.; Wang, S.; Wang, Z. Recent advance on carbamate-based cholinesterase inhibitors as potential multifunctional agents against Alzheimer's disease. *Eur. J. Med. Chem.* **2022**, *240*, 114606, https://doi.org/10.1016/j.ejmech.2022.114606.
11. Kant, R.; Maji, S. Recent advances in the synthesis of piperazine based ligands and metal complexes and their applications. *Dalton Trans.* **2021**, *50*, 785-800, https://doi.org/10.1039/D0DT03569F.
12. Ostermeier, M.; Limberg, C.; Ziemer; B. The Coordination Chemistry of Iron with the 1,4-Bis(2-pyridyl-methyl)piperazine Ligand. *Z. Anorg. Allg. Chem.* **2006**, *632*, 1287-1292, https://doi.org/10.1002/zaac.200600003.
13. Höpfl, H.; Farfán, N.; Castillo, D.; Santillan, R.; Gutierrez, A.; Daran, J.C. Study of cyclic borinates obtained from piperidine-and piperazine alcohols by spectroscopic methods and X-ray crystallography. *J. Organomet. Chem.* **1998**, *553*, 221-239, https://doi.org/10.1016/S0022-328X(97)00636-0.

14. Ibrahim, S.A.; Ragab, A.; El-Ghamry, H.A. Coordination compounds of pyrazolone-based ligand: Design, characterization, biological evaluation, antitumor efficiency, and DNA binding evaluation supported by in silico studies. *Appl. Organomet. Chem.* **2022**, *36*, e6508, https://doi.org/10.1002/aoc.6508.
15. Abdel-Rahman, L.H.; Al–Farhan, B.S.; Al Zamil, N.O.; Noamaan, M.A.; Ahmed, H.E.S.; Adam, M.S.S., Synthesis, spectral characterization, DFT calculations, pharmacological studies, CT-DNA binding and molecular docking of potential N, O-multidentate chelating ligand and its VO(II), Zn(II) and ZrO(II) chelates. *Bioorg. Chem.* **2021**, *114*, 105106, https://doi.org/10.1016/j.bioorg.2021.105106.
16. Pait, M.; Kundu, B.; Kundu, S.C.; Ray, D. Copper(II) complexes of piperazine based ligand: Synthesis, crystal structure, protein binding and evaluation of anti-cancerous therapeutic potential. *Inorganica Chim. Acta* **2014**, *418*, 30-41, https://doi.org/10.1016/j.ica.2014.04.019.
17. Singh, A.; Prasad, L.B.; Shiv, K.; Kumar, R.; Garai, S. Synthesis, characterization, and in vitro antibacterial and cytotoxic study of Co(II), Ni(II), Cu(II), and Zn(II) complexes of N-(4-methoxybenzyl) N-(phenylethyl) dithiocarbamate ligand. *J. Mol. Struct.* **2023**, *1288*, 135835, https://doi.org/10.1016/j.molstruc.2023.135835.
18. Aggarwal, N.; Kant, R.; Kumar, G.; James, C.; Maji, S. Synthesis, characterization and biological evaluation studies of Cu(II) and Zn(II) complexes with gly-*o*-andn or gly-*p*-andn as primary ligand and N, N' donors as secondary ligand. *J. Phys.: Conf. Ser.* **2020**, *1531*, 012111, https://doi.org/10.1088/1742-6596/1531/1/012111.
19. Ganot, N.; Meker, S.; Reytman, L.; Tzubery, A.; Tshuva, E.Y. Anticancer Metal Complexes: Synthesis and Cytotoxicity Evaluation by the MTT Assay. *JoVE (J. Vis. Exp.)* **2013**, *81*, e50767, https://doi.org/10.3791/50767.
20. Keypour, H.; Azizi, E.; Mahmoudabadi, M.; Salehzadeh, S.; Hajibabaei, F.; Gable, R.W. Synthesis and crystal structure of manganese(III), zinc(II) and cadmium(II) complexes based on a symmetrical macroacyclic Schiff base ligand containing piperazine moiety, DNA binding studies of complexes. *Transit. Met. Chem.* **2020**, *45*, 227-235, https://doi.org/10.1007/s11243-019-00374-8.
21. Raghi, K.R.; Sherin, D.R.; Archana, T.M.; Saumya, M.J.; Sajesha, K.P.; Manojkumar, T.K. Identification of Potent ABL Inhibitors from Coumestrol: An Integrative *In Silico* Approach. *J. Comput. Biophys. Chem.* **2022**, *21*, 967-979, https://doi.org/10.1142/S2737416522500429.
22. Bhat, I.-u.-H.; Tabassum, S. Synthesis of new piperazine derived Cu(II)/Zn(II) metal complexes, their DNA binding studies, electrochemistry and antimicrobial activity: Validation for specific recognition of Zn(II) complex to DNA helix by interaction with thymine base. *Spectrochim. Acta A: Mol. Biomol. Spectrosc.* **2009**, *72*, 1026-1033, https://doi.org/10.1016/j.saa.2008.12.037.
23. Alaghaz, A.-N.M.A.; Ammar, R.A. New dimeric cyclodiphosph(V)azane complexes of Cr(III), Co(II), Ni(II), Cu(II), and Zn(II): Preparation, characterization and biological activity studies. *Eur. J. Med. Chem.* **2010**, *45*, 1314-1322, https://doi.org/10.1016/j.ejmech.2009.12.008.
24. Alaghaz, A.-N.M.A.; El-Sayed, B.A.; El-Henawy, A.A.; Ammar, R.A.A. Synthesis, spectroscopic characterization, potentiometric studies, cytotoxic studies and molecular docking studies of DNA binding of transition metal complexes with 1,1-diaminopropane–Schiff base. *J. Mol. Struct.* **2013**, *1035*, 83-93, https://doi.org/10.1016/j.molstruc.2012.09.032.
25. Dong, W.-K.; Sun, Y.-X.; Zhang, Y.-P.; Li, L.; He, X.-N.; Tang, X.-L. Synthesis, crystal structure, and properties of supramolecular Cu^{II}, Zn^{II}, and Cd^{II} complexes with Salen-type bisoxime ligands. *Inorganica Chim. Acta* **2009**, *362*, 117-124, https://doi.org/10.1016/j.ica.2008.03.128.
26. Chandra, S.; Jain, D.; Sharma, A.K. EPR, mass, electronic, IR spectroscopic and thermal studies of bimetallic copper(II) complexes with tetradentate ligand, 1,4-diformyl piperazine bis(carbohydrazone). *Spectrochim. Acta A: Mol. Biomol. Spectrosc.* **2009**, *71*, 1712-1719, https://doi.org/10.1016/j.saa.2008.06.028.
27. Mahmoud, W.H.; Deghadi, R.G.; Mohamed, G.G. Preparation, geometric structure, molecular docking thermal and spectroscopic characterization of novel Schiff base ligand and its metal chelates: Screening their anticancer and antimicrobial activities. *J. Therm. Anal. Calorim.* **2017**, *127*, 2149-2171, https://doi.org/10.1007/s10973-016-5826-7.
28. Hemalatha, S.; Dharmaraja, J.; Shobana, S.; Subbaraj, P.; Esakkidurai, T.; Raman, N. Chemical and pharmacological aspects of novel hetero MLB complexes derived from NO_2 type Schiff base and N_2 type 1,10-phenanthroline ligands. *J. Saudi Chem. Soc.* **2020**, *24*, 61-80, https://doi.org/10.1016/j.jscs.2019.09.004.
29. Saadeh, S.M. Synthesis, characterization and biological properties of Co(II), Ni(II), Cu(II) and Zn(II) complexes with an SNO functionalized ligand. *Arab. J. Chem.* **2013**, *6*, 191-196, https://doi.org/10.1016/j.arabjc.2010.10.002.
30. Liu, Z.-Q.; Ng, Y.-M.; Tiong, P.J.; Abu Talip, R.A.; Jasin, N.; Jong, V.Y.M.; Tay, M.G. Five-Coordinate Zinc(II) Complex: Synthesis, Characterization, Molecular Structure, and Antibacterial Activities of Bis-[(*E*)-

2-hydroxy-*N'*-{1-(4-methoxyphenyl)ethylidene}benzohydrazido]dimethylsulfoxidezinc(II) Complex. *Int. J. Inorg. Chem.* **2017**, *2017*, 7520640, https://doi.org/10.1155/2017/7520640.

31. Ali, I.; Wani, W.A.; Saleem, K. Empirical Formulae to Molecular Structures of Metal Complexes by Molar Conductance. *Synth. React. Inorg. Met.-Org., Nano-Met. Chem.* **2013**, *43*, 1162-1170, https://doi.org/10.1080/15533174.2012.756898.
32. Aggoun, D.; Fernández-García, M.; López, D.; Bouzerafa, B.; Ouennoughi, Y.; Setifi, F.; Ourari, A. New nickel (II) and copper (II) bidentate Schiff base complexes, derived from dihalogenated salicylaldehyde and alkylamine: Synthesis, spectroscopic, thermogravimetry, crystallographic determination and electrochemical studies. *Polyhedron* **2020**, *187*, 114640, https://doi.org/10.1016/j.poly.2020.114640.
33. Eğlence-Bakır, S. New nickel(II) complexes containing N_2O_2 donor thiosemicarbazones: Synthesis, characterization and antioxidant properties. *J. Mol. Struct.* **2021**, *1246*, 131121, https://doi.org/10.1016/j.molstruc.2021.131121.
34. Kant, R.; Saini, R.; Kaur, M.; Karnwal, A.; Rather, H.A.; Maji, S. Synthesis and characterization of copper complexes of phenylpiperazine ring-based ligands and evaluation of their antimicrobial, BSA binding, computational, and molecular docking studies. *J. Phys.: Conf. Ser.* **2022**, *2267*, 012154, https://doi.org/10.1088/1742-6596/2267/1/012154.
35. Neese, F. The ORCA program system. *Wiley Interdiscip. Rev. Comput. Mol. Sci.* **2012**, *2*, 73-78, https://doi.org/10.1002/wcms.81.
36. Trott, O. Olson, A.J., AutoDock Vina: Improving the speed and accuracy of docking with a new scoring function, efficient optimization, and multithreading. *J. Comput. Chem.* **2009**, *31*, 455-461, https://doi.org/10.1002/jcc.21334.

Supplementary materials

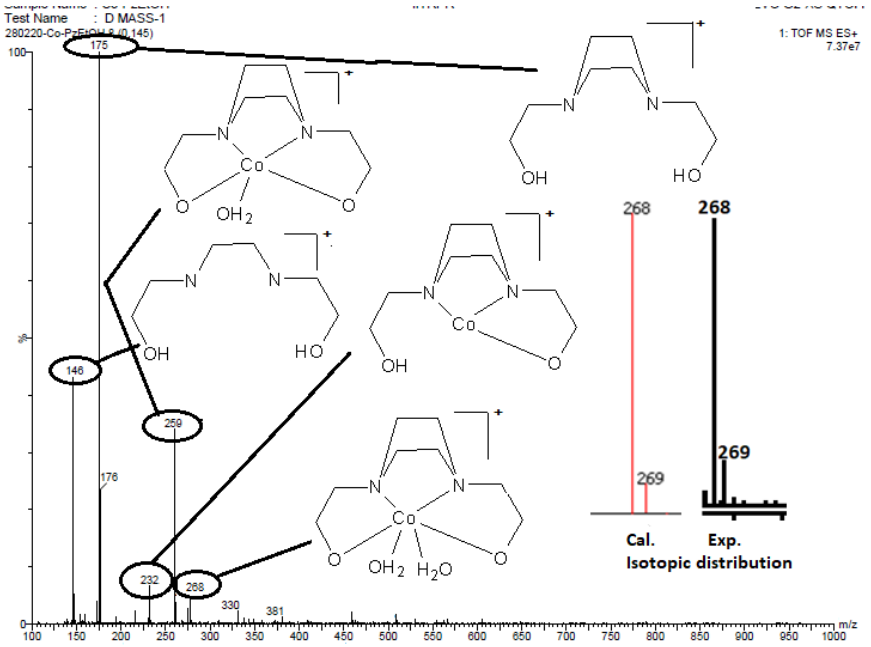

Figure S1. Mass spectra of CoL1.

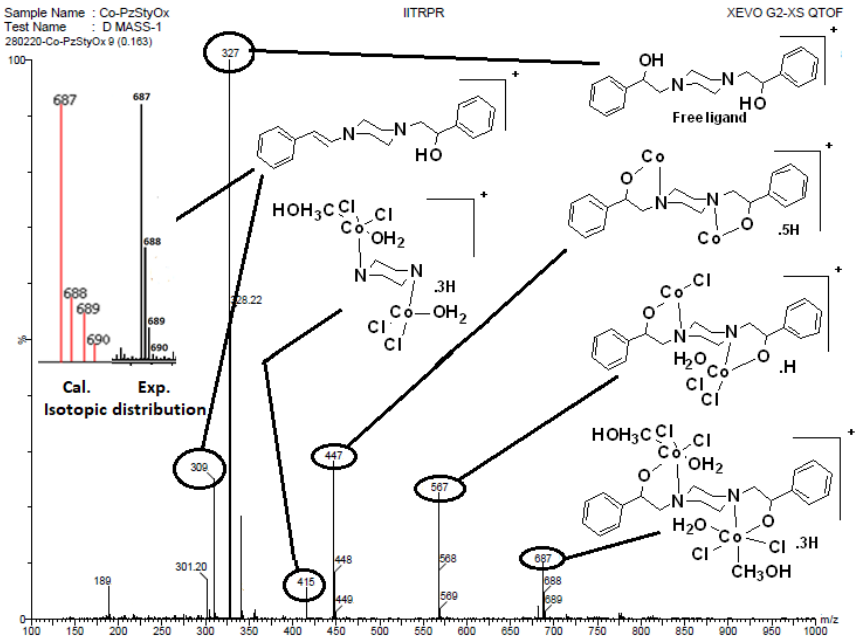

Figure S2. Mass spectra of Co_2L2.

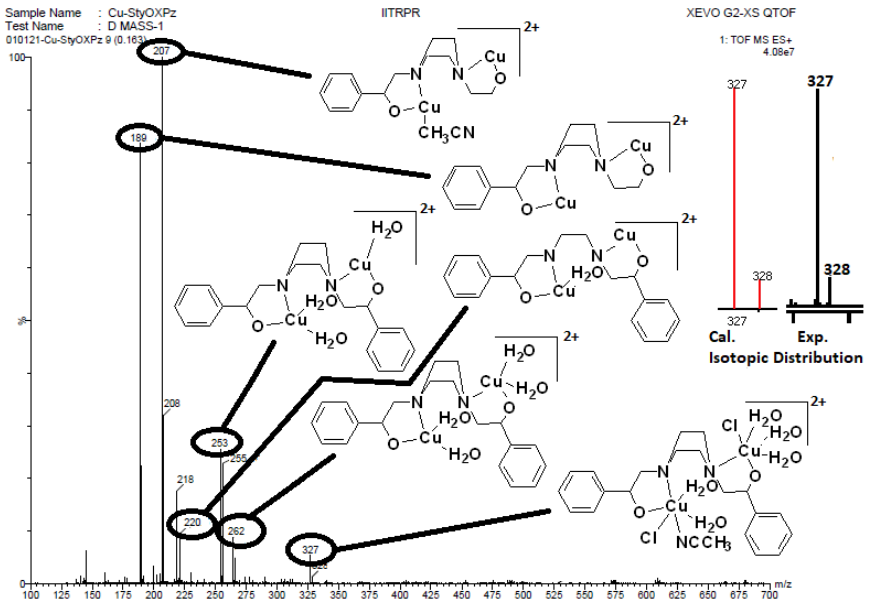

Figure S3. Mass spectra of Cu_2L2.

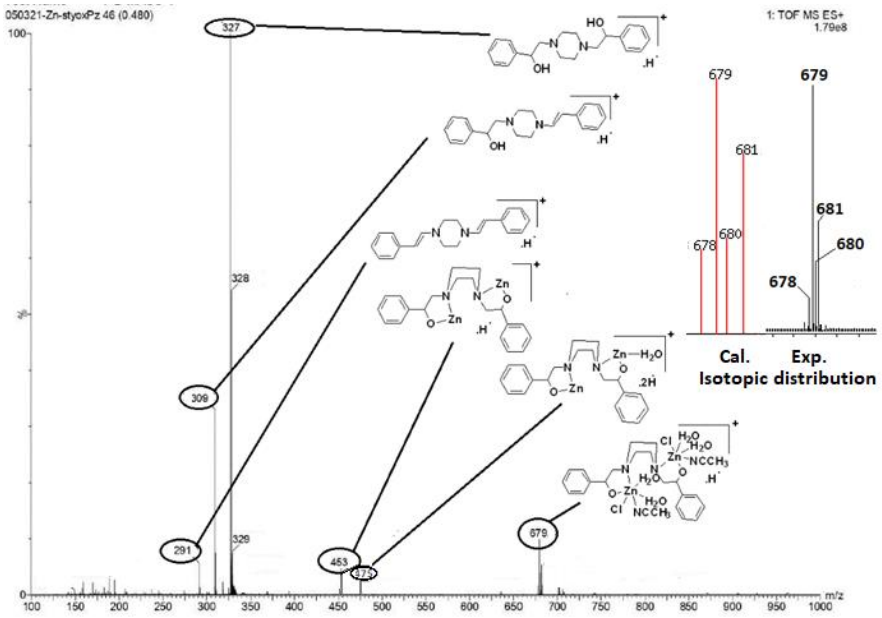

Figure S4. Mass spectra of Zn_2L2.

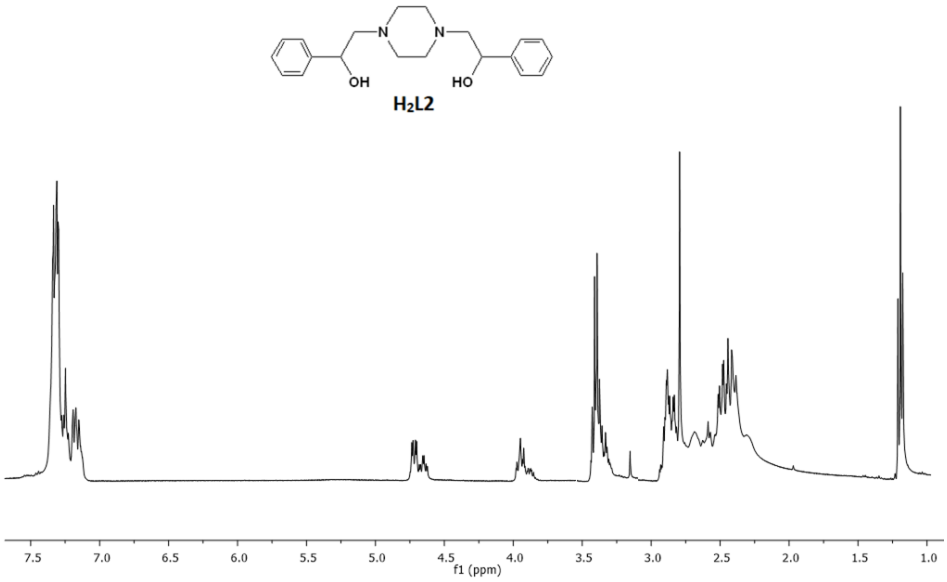

Figure S5. NMR spectra of H_2L2.

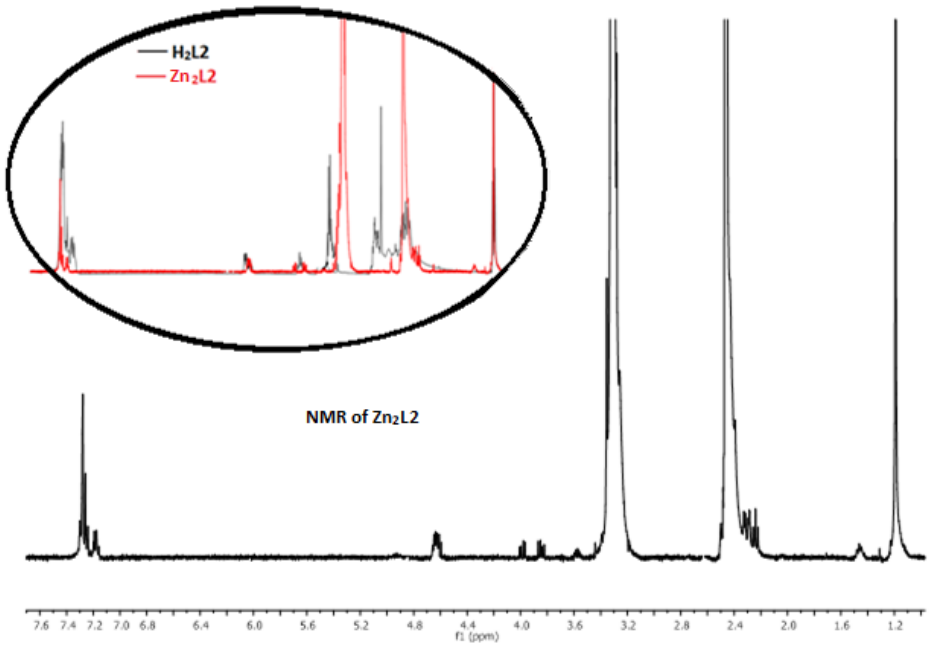

Figure S6. NMR spectra of Zn_2L2.

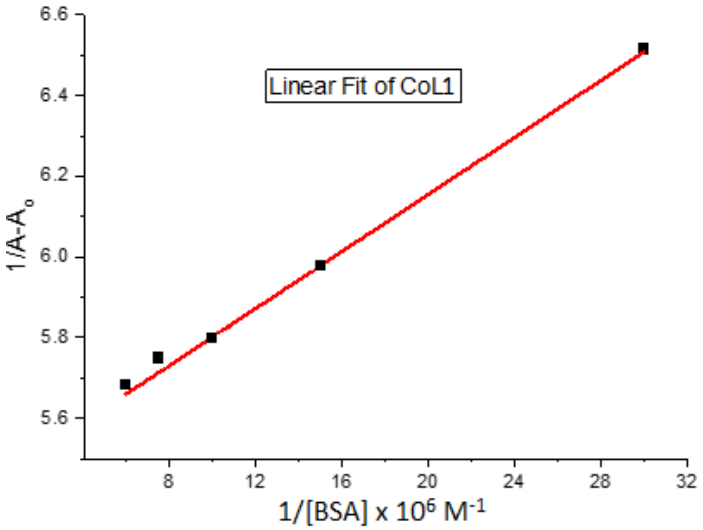

Figure S7. Linear fit graph of CoL1 used in BSA binding constant.

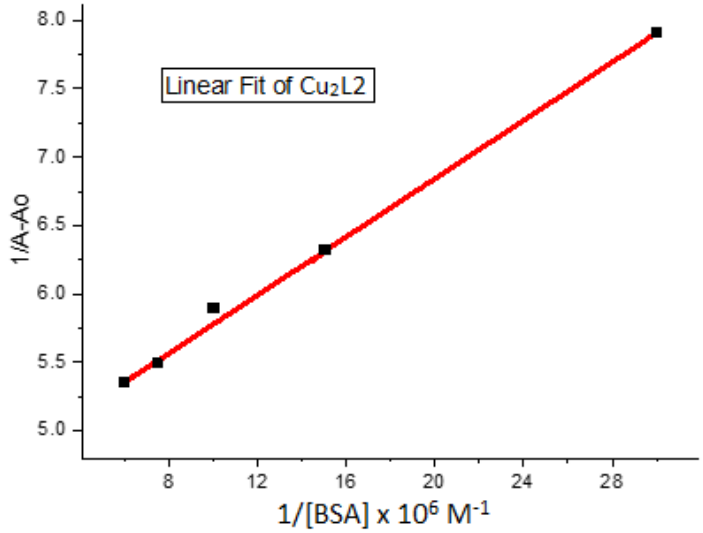

Figure S8. Linear fit graph of Co_2L2 used in BSA binding constant.

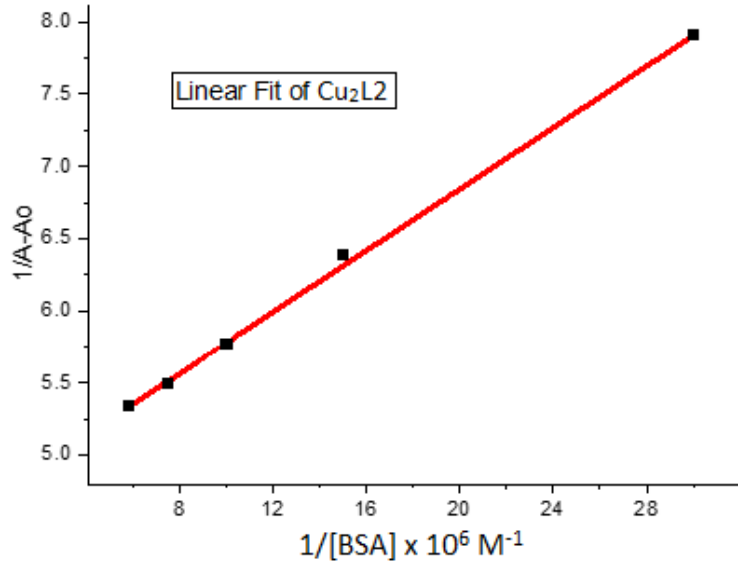

Figure S9. Linear fit graph of Cu_2L2 used in BSA binding constant.

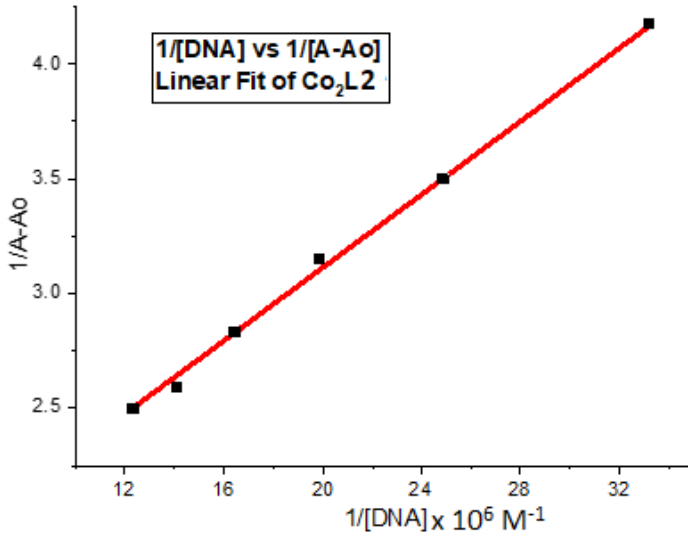

Figure S10. Linear fit graph of Co_2L2 used in DNA binding constant.

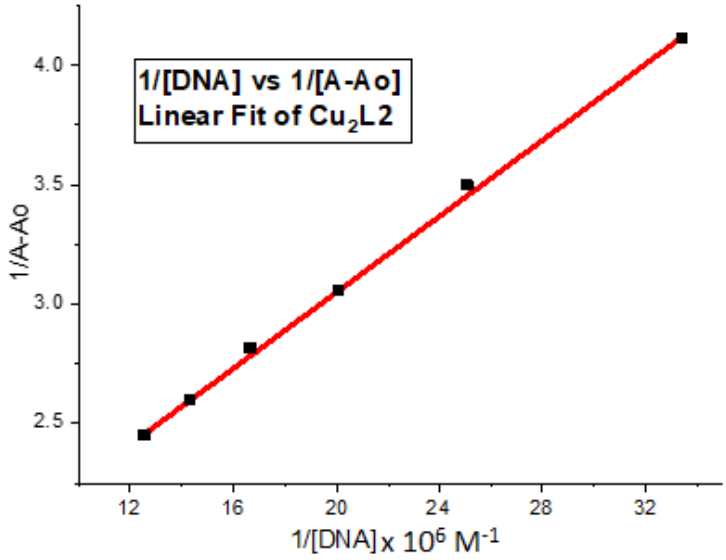

Figure S11. Linear fit graph of Cu_2L2 used in DNA binding constant.

Table S1. Optimized geometry coordinates of ligand H_2L1.

Atom	x	y	z
C	-0.68621	1.072155	0.435649
C	0.735928	1.379675	-0.10954
H	0.605883	2.029001	-0.97697
H	1.330431	1.918195	0.630279
H	-0.53739	0.544227	1.379065
H	-1.23967	1.991544	0.631917
N	1.360216	0.246148	-0.51968
C	0.684653	-0.57993	-1.35874
H	1.241869	-1.49834	-1.55054
H	0.548029	-0.06165	-2.30938
C	-0.73562	-0.89378	-0.81267
H	-0.58486	-1.52697	0.063248
H	-1.32699	-1.44388	-1.54597

Atom	x	y	z
N	-1.35319	0.245044	-0.40841
C	-2.68028	0.399962	-0.59917
H	-2.95648	1.455503	-0.56905
H	-2.98952	-0.06939	-1.5342
C	-3.42683	-0.31779	0.53861
H	-2.91278	-1.23093	0.841788
H	-4.40616	-0.61604	0.164127
O	-3.61001	0.380349	1.53526
H	-4.02265	-0.26512	2.853811
C	2.708007	0.228075	-0.54655
H	3.126938	1.232915	-0.46424
H	3.087283	-0.2849	-1.43254
C	3.155707	-0.56853	0.683695
H	2.777938	-0.09805	1.592509
H	2.739546	-1.57631	0.649279
O	4.377232	-0.66427	0.784036
H	4.988975	-1.42692	1.954379

Table S2. Optimized geometry coordinates of ligand H_2L2.

Atom	x	y	z
C	0.307282	0.661938	-0.40498
C	1.729424	0.969462	-0.95016
H	1.599378	1.618791	-1.8176
H	2.323926	1.507979	-0.21034
H	0.456107	0.134006	0.538436
H	-0.24617	1.581326	-0.20871
N	2.353712	-0.16406	-1.36031
C	1.67815	-0.99014	-2.19937
H	2.235367	-1.90855	-2.39118
H	1.541526	-0.47186	-3.15001
C	0.257879	-1.30399	-1.6533
H	0.408633	-1.93718	-0.77739
H	-0.33349	-1.85409	-2.38661
N	-0.35969	-0.16517	-1.24904
C	-1.68678	-0.01025	-1.4398
H	-1.96298	1.045288	-1.40968
H	-1.99602	-0.4796	-2.37483
C	-2.43333	-0.728	-0.30202
H	-3.41266	-1.02626	-0.67651
O	-2.61652	-0.02988	0.694629
H	-3.02915	-0.67535	2.013178
C	3.701503	-0.18214	-1.38718
H	4.120434	0.822705	-1.30486
H	4.08078	-0.69511	-2.27318
C	4.149204	-0.97874	-0.15694
H	3.733043	-1.98652	-0.19136

Atom	x	y	z
O	5.370729	-1.07449	-0.0566
H	5.982472	-1.83714	1.113743
C	3.670132	-0.35945	1.163049
C	2.576288	-1.07705	1.956542
H	2.152754	-2.01343	1.593191
C	2.070082	-0.456	3.259655
H	1.287276	-0.95355	3.83197
C	2.661031	0.86663	3.758856
H	2.29755	1.306683	4.687387
C	3.759815	1.574232	2.958818
H	4.175108	2.515594	3.318361
C	4.271095	0.962278	1.653191
H	5.046738	1.46627	1.076481
C	-3.8922	-0.04074	-0.2752
C	-4.38071	1.01038	-1.32547
H	-3.73632	1.377657	-2.12059
C	-5.80815	1.561949	-1.2932
H	-6.11124	2.310006	-2.02567
C	-6.81974	1.063927	-0.26541
H	-7.83384	1.463356	-0.25982
C	-6.42396	-0.02752	0.722079
H	-7.15684	-0.40953	1.432647
C	-5.00634	-0.59639	0.709825
H	-4.75123	-1.38801	1.415221

Table S3. Optimized geometry coordinates of complex CoL1.

Atom	x	y	z
C	1.088098	-1.77008	0.950791
C	-0.41694	-1.76095	1.391815
H	-0.78883	-2.79078	1.536948
H	-0.5212	-1.20734	2.327386
H	1.694003	-1.2491	1.695754
H	1.468613	-2.80286	0.857457
N	-1.19425	-1.04789	0.34528
C	-1.0881	-1.77091	-0.9492
H	-1.69383	-1.2504	-1.69462
H	-1.46874	-2.80358	-0.85516
C	0.416968	-1.76228	-1.39013
H	0.521236	-1.20969	-2.32629
H	0.788888	-2.79227	-1.53405
N	1.194209	-1.04808	-0.34431
C	2.543108	-0.56782	-0.73236
H	3.306284	-1.36724	-0.69365
H	2.464568	-0.22132	-1.76943
C	2.956594	0.626197	0.172188
H	3.794409	1.151438	-0.31461

Atom	x	y	z
H	3.333656	0.246893	1.140368
O	1.848595	1.518926	0.382103
C	-2.54309	-0.56708	0.732916
H	-2.46441	-0.21948	1.769611
H	-3.30635	-1.36645	0.695114
C	-2.9565	0.626053	-0.17282
H	-3.79431	1.151818	0.313406
H	-3.33348	0.245872	-1.14068
O	-1.84844	1.518573	-0.38351
Cu	0.000004	0.794063	-0.00019
O	0.223726	1.25243	2.140897
O	-0.22394	1.248837	-2.1425
H	-0.32165	2.004238	2.442304
H	0.321166	2.000459	-2.44491
H	1.130486	1.542891	1.688157
H	-1.13064	1.54012	-1.68997

Table S4. Optimized geometry coordinates of complex Cu_2L2.

Atom	x	y	z
C	-0.60493	-0.79908	1.396777
C	0.492511	0.306913	1.420383
H	0.023273	1.293912	1.483146
H	1.149722	0.18917	2.288334
H	-0.14364	-1.79	1.352282
H	-1.21876	-0.74846	2.300374
N	1.32298	0.258138	0.188989
C	0.483706	0.367251	-1.03001
H	1.109461	0.236198	-1.91747
H	0.073424	1.379858	-1.0847
C	-0.66653	-0.69513	-1.04714
H	-0.25474	-1.70381	-1.13671
H	-1.30575	-0.50415	-1.91581
N	-1.49242	-0.65516	0.198954
C	-2.40689	0.548009	0.273113
H	-2.67956	0.692143	1.323116
H	-1.89859	1.453447	-0.08666
C	-3.69967	0.255658	-0.52234
H	-3.44378	0.175268	-1.59681
O	-4.22238	-0.97921	-0.01531
C	2.308858	-0.88002	0.159665
H	2.471761	-1.20795	1.189428
H	1.919365	-1.72838	-0.41868
C	3.655138	-0.3708	-0.42099
H	3.512799	-0.11784	-1.48417
O	3.999427	0.832063	0.302222
C	4.767049	-1.4035	-0.3137
C	5.343033	-1.95729	-1.47556
H	4.998699	-1.62695	-2.45397
C	6.366408	-2.9192	-1.38126
H	6.802857	-3.33805	-2.28519
C	6.829328	-3.33306	-0.11753

Atom	x	y	z
H	7.6223	-4.07379	-0.04142
C	6.264409	-2.77723	1.048358
H	6.623483	-3.08969	2.026537
C	5.240228	-1.81953	0.952752
H	4.816794	-1.38511	1.85546
C	-4.71016	1.390468	-0.37104
C	-5.60547	1.394185	0.719122
H	-5.59869	0.551227	1.404191
C	-6.51624	2.453401	0.888175
H	-7.20763	2.443824	1.727932
C	-6.54267	3.52062	-0.03187
H	-7.25109	4.336145	0.095704
C	-5.65759	3.517156	-1.12843
H	-5.68454	4.329099	-1.85179
C	-4.7493	2.454853	-1.29718
H	-4.08073	2.447176	-2.15735
Cu	-2.82765	-2.31848	0.199182
Cu	2.608437	2.132216	0.091126
Cl	-1.07679	-4.01765	-0.03162
O	-2.84323	-3.10776	2.384713
H	-3.75504	-3.45992	2.413518
O	-4.4334	-3.53147	-0.31347
H	-4.15319	-4.06246	-1.12603
O	-3.18836	-4.74334	-2.14076
H	-3.28976	-5.43868	-2.81084
H	-2.21163	-3.82638	2.150333
H	-5.01617	-2.76501	-0.51569
H	-2.32497	-4.76428	-1.65845
Cl	2.629538	2.888979	-2.27588
O	4.050869	3.902749	0.161219
O	3.355086	0.61975	2.830208
H	4.50014	4.664455	0.56823
H	3.885079	1.097991	3.494883
H	3.732594	0.733654	1.896761
H	4.005959	3.93316	-0.82843
C	-0.23731	5.727445	0.621728
C	0.503403	4.465466	0.647904
H	0.42819	6.540977	0.312631
H	-0.64373	5.958473	1.612395
H	-1.06521	5.663584	-0.09291
N	1.115684	3.46534	0.634953